Int. J. Electrochem. Sci., 10 **(2015)** 4985 - 5000

International Journal of
ELECTROCHEMICAL
SCIENCE
www.electrochemsci.org

Comparing Electrochemical Behaviour of Amorphous Ni–P Powders and Film

H. Xu[1], *S. L*[1], *L.Y. Guo*[1], *Y.J. Li*[1], *K.C. Shen*[1], *C.S. Guan*[2], *W.M. Wang* [1,*]

[1] Key Laboratory for Liquid-Solid Structural Evolution and Processing of Materials, Ministry of Education, Shandong University, Jinan 250061, China
[2] College of Chemical Science and Engineering, Ministry of Education, Shandong University, Jinan 250061, China
[*]E-mail: weiminw@sdu.edu.cn

Received: 10 March 2015 / *Accepted:* 29 March 2015 / *Published:* 28 April 2015

Nickel-phosphorous (Ni–P) powders and films were prepared by electroless deposition on copper particle and brass substrate and investigated with different techniques. Microstructure investigations show that powder sample owns a more developed porous microstructure and a higher amorphous fraction than film sample. The potentiodynamic polarization analysis reveals that the Ni–P powders own the better corrosion resistance ability compared with film, which agrees with the results of the Electrochemical Impedance Spectroscopy (EIS). The Mott-Schottky approach indicates a lower conductive behaviour of Ni–P powder sample compared with film sample. Cyclic voltammetry tests indicate that Ni–P powders exhibit a higher catalytic activity for electro-oxidation of ethanol in alkaline solution.

Keywords: Amorphous Ni–P, Corrosion, Electrochemical impedance, Electrocatalyst.

1. INTRODUCTION

The amorphous alloys, also called metallic glasses, owing to their good magnetic, mechanical, catalytic properties and corrosion resistance, have attracted the interest of many researchers for decades [1]. For example, ferrous-group-based glasses had been widely applied to transformer component [2]. Electroless Ni–P coatings, firstly developed by Brenner and Riddell, have been extensively used in mechanical, chemical and electronic industries [3]. Ni–P coatings can be prepared by electroless deposition from the solution containing metal ions, reducing agents, operating in a specific temperature and pH ranges [4, 5]. And a phosphorous compound shows excellent properties such as bright appearance, high hardness, outstanding wear and corrosion resistance, good mechanical

properties as well as catalytic properties due to its amorphous microstructure [6-9]. Amorphous is an unstable states and it has the trends to be crystalline phase under high temperature and press. Lu. et al. [10] have studied the physical properties of nanocrystalline Ni–P ribbons. It is interesting to study the microstructure comparison between Ni–P powders and film.

The electrochemical properties of the electroless Ni–P alloy can be controlled by tuning the content of phosphorous in the deposition [11]. The Ni–P coatings composition depends on the bath composition, pH values and temperature of solution. The microstructure of them depends on the method of preparation (electro- or electroless deposition) and P content [12]. Electroless Ni–P is the barrier coating which protects the substrate by sealing it from the environment. The corrosion resistances of the coatings are excellent due to its amorphous nature and passivity [13]. Passive films formed on amorphous Ni–P electrodes in the corrosion process show a semiconductive behaviour, which might be related to their corrosion resistance. It is essential to assess their electronic properties to obtain a better understanding of the electrochemical behaviour of the surface films. The Mott-Schottky test has been widely used and it is a valid method to measure the semiconductive character like the acceptor and donor density in the surface film [14]. However, to the authors' knowledge, there is rarely report on the relationship between the semiconductive behaviour and corrosion resistance of Ni–P powders and film.

Ni–contained electrocatalysts for alcohol oxidation have been an promising and widespread commercial use due to its high efficiency, low cost, environmental friendly and simplicity preparation [15-17]. Moreover, Nickel-based alloys have been one cheap catalyst to improve the oxidation efficiency in the alcohol oxidation. It has been demonstrated that in alkaline medium the polar organic compounds can be anodic oxidized by pure Ni electrode. Porous materials such as Ni–P powders present an excellent catalysis for ethanol oxidation in alkaline solution own to numeric pores and cavities in the range of molecular dimensions as well as channels formed in the interior of microstructure [18, 19]. Fleischmann et al. explained the alcohols oxidation mechanism of Ni electrode involving electron transfer mediation by $Ni(OH)_2$/NiOOH redox couple in the oxide film [19, 20]. It is meaningful to compare the electrocatalytic feature of Ni–P powders with that of film.

In this paper, we chose copper powders (with a diameter of 60 μm) and brass sheet as substrates for electroless deposition. The microstructure, morphology, corrosion resistance, semiconductor feature and catalytic properties and relationship between these behaviours were investigated.

2. EXPERIMENTAL

2.1 Electroless deposition

Table 1 shows the bath compositions and operating conditions for preparing Ni–P coatings. Before electroless deposition, the brass substrates were cut into 3×5 cm areas, and polished to mirror finish with 3000 grit SiC paper, mechanically. And then the pure copper particles and brass substrates are subjected to the pretreatment process. Firstly they were degreased in the 30 % NaOH solution for

10 min, rinsed thoroughly with distilled water, acetone immersing and deionized water cleaning as follows, at last, dried in air.

Table 1. Chemical composition and operating conditions of the electroless nickel deposition bath.

Bath composition		Deposition condition	
Component	Concentration	Parameter	Value
Nickel sulfate	25 g/L	pH	5±0.1
Natrium aceticum	12 g/L	Temperature	85±1.0℃
Lactic acid	28 ml/L	Deposition during	1 h
Sodium hypophosphite	25 g/L	Deposition rate	38 μm/h

Ni–P powders were prepared by electroless deposition using pure copper particles (with a diameter of 60 μm) as substrates. The Ni–P powders were made as electrodes: (1) a certain amount of 1×1 cm areas nickel foam was selected as electrode substrate, which should be degreased in 35 % HCl solution and cleaned in distilled water for 3 or 4 times; (2) the mass proportion of the specimen pulverized into ultrafine powders with agate mortar combined with polyvinylidene fluoride (PVDF) and graphite is 8:1:1; (3) then they were mixed into black mixture with N-methyl-2-pyrrolidone, stirring fully with the magnetic stirrer; (4) at last, we put nickel foam into the mixture, transferred the foam covered with the mixture into drying oven at 90 ^{0}C for 8 h.

2.2 Microstructure and morphology characterization

The phases of the samples were characterized using an X-ray diffractometer with Cu Kα radiation in the 2θ range from 10 to 90 degree. The morphological images of original Ni–P alloy and specimen after potentiodynamic polarization were obtained by scanning electron microscopy (SEM). And transmission electron microscopy (TEM) was used to observe atomic microstructure.

2.3 Electrochemical test

Electrochemical experiments were performed in a three-electrode cell using an electrochemistry work station (CHI660E, Chenhua instrument Ltd., Shanghai) at 25 ^{0}C. A typical three-electrode system was obtained in these measurements: the working electrode was stationary specimen, a Pt foil was used as the counter electrode and the Hg/HgCl electrode filled with saturation KCl solution (SCE) was used as the reference electrode. We also used the Hg/HgO electrode filled with 1 M NaOH solution as reference electrode for testing corrosion properties in alkaline solution. Tafel tests were performed in a 3.5 wt% NaCl aqueous solution and 1 M NaOH solution respectively in the range from -1.8 to 1.8 V. The parameters of the Tafel tests were obtained from the fitting function of CHI 660E. The electrochemical impedance spectroscopy (EIS) of Ni–P alloys was

performed after open-circuit potential (OCP) tests in 1 M NaOH solution for 120 min until the open-circuit potentials were steady. Data fitting and elements analysis were performed by using the ZSimpwin simulating software. The Mott-Schottky tests were carried out in 1 M NaOH solution with the potential from -1.0 to 0.2 V. The impedance was recorded at 1000 Hz frequency to avoid the frequency dispersion in Mott-Schottky tests. The cycle voltammetric behaviour was characterized in solutions of 1.0 M NaOH; 1 M NaOH in the presence of 1 M ethanol. In order to obtain the electrochemical data with the same condition, all the electrochemical tests used a constant scan rate of 5 mV/s.

3. RESULTS AND DISCUSSION

3.1. Microstructure and morphology

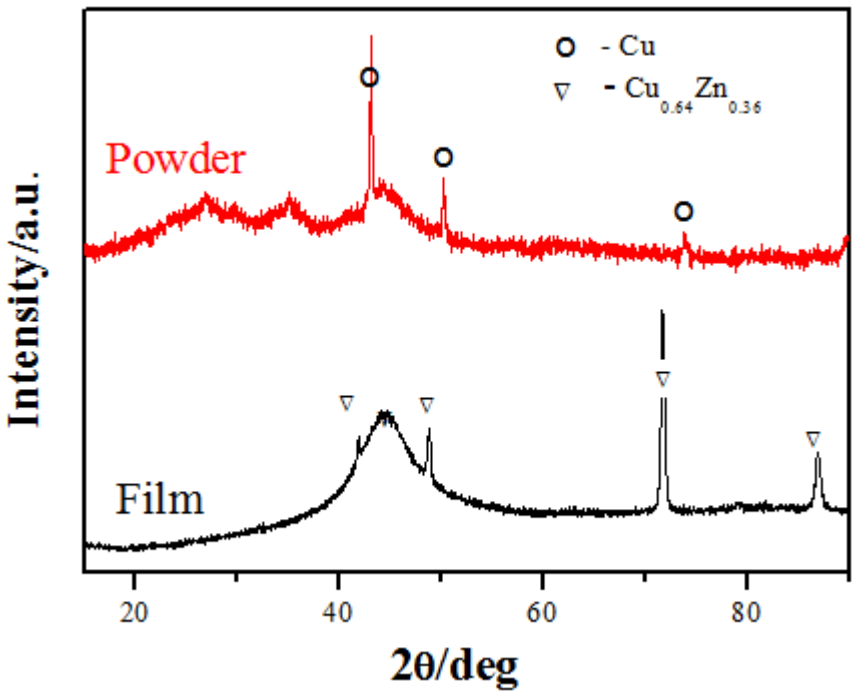

Figure 1. XRD patterns of powder and film samples.

Fig. 1 shows the XRD patterns of Ni–P alloy, revealing the characteristic broad diffraction peaks from 20 to 40 degree (2θ), and no visible diffraction peaks corresponding to crystalline phases except obviously sharp peaks from substrates Cu and $Cu_{0.64}Zn_{0.36}$ for powders and film, respectively. Based on the intensity of substrate phases, the fraction of amorphous phase f_a of powders is higher than that of film. Different from Georgiza's work [21], no nanocrystalline nickel phase is revealed in our XRD patterns.

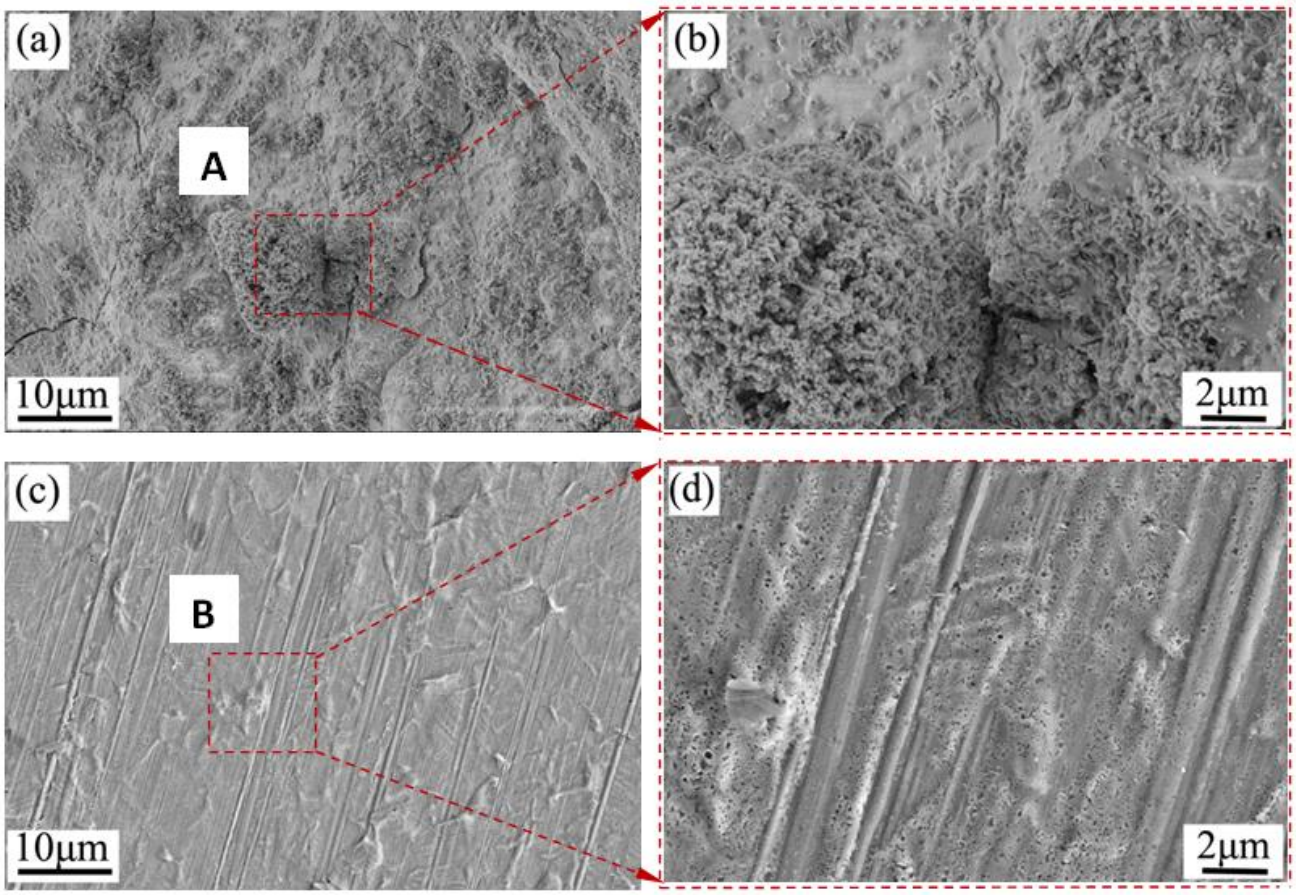

Figure 2. SEM images of powder sample (a and b) and film sample (c and d). EDS of A point: c_P = 16.72 at%, B point: c_P = 8.9 at%.

The surface morphology of Ni–P powders and film can be observed in Fig. 2. Dense base covered by the particles in the size of 50 nm to 400 nm as well as thin aggregates can be observed in the surface of the Ni–P powder sample (Fig. 2a and b); the whole morphology of Ni–P film is smooth or with a lower surface roughness except some stripe-like folds and tiny holes, resulting from the inhomogeneity of electroless deposition (Fig. 2c and d). Energy Dispersive Spectrometer (EDS) shows that the phosphorus content of Ni–P powders or film is respectively 16.7 % or 8.9 %.

Fig. 3 exhibits the TEM bright field images and corresponding selected area diffraction (SAED) patterns of both samples. The bright field image of the powder sample shows a maze-like pattern with separated round dark zones in size of about 5 nm (Fig. 3a). There exist a typical amorphous halo in the SAED pattern (Fig. 3b), which is corresponding with the atomic arranging pattern in its bright filed images. Besides, there present crystalline spots indexed as $Ni_{12}P_5$, which agrees well with the results of the work of Yu et al. [22].

In the bright field image of film (Fig. 3c), a series of mutual parallel stripes contains regular arraying atoms beneath the maze-like atomic pattern. In the corresponding SAED (Fig. 3d), the amorphous halo is much slighter than that in case of powder sample, and the spots can be indexed as $Ni_{12}P_5$ as well as the substrate phase $Cu_{0.64}P_{0.36}$.

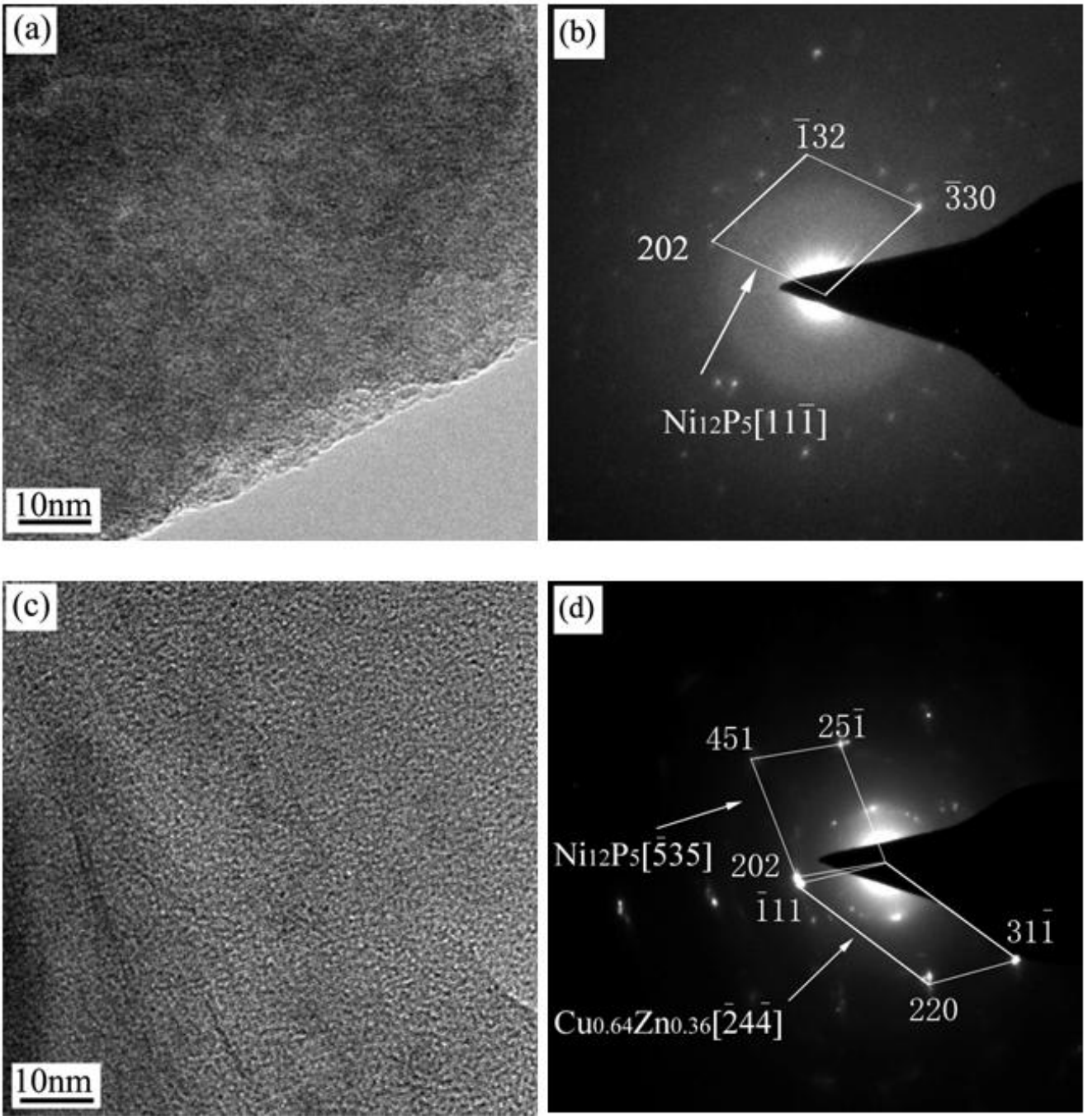

Figure 3. TEM images and the corresponding selected area electron diffraction (SAED) patterns of (a) powder sample, and (c) film sample. (b) and (d) are SAED patterns of (a) and (c) , respectively.

In addition, the bright area of the spots of film sample is higher than that of powder sample. It should be pointed out that the crystalline phases identified by TEM reflect the local microstructure of the sample [23]. The fact that the identified crystalline phases are not shown in XRD pattern is owing to the lower fraction of crystallites or the crystallites formation in TEM sample thinning.

3.2. Corrosion behaviour

Fig. 4 shows the potentiodynamic polarization curves of the Ni–P powders and film in 3.5 wt% NaCl and 1 M NaOH solutions. In 3.5 wt% NaCl solution, the powder sample has a corrosion potential E_{corr} of -0.66 V_{sce}, more positive than that of film sample.

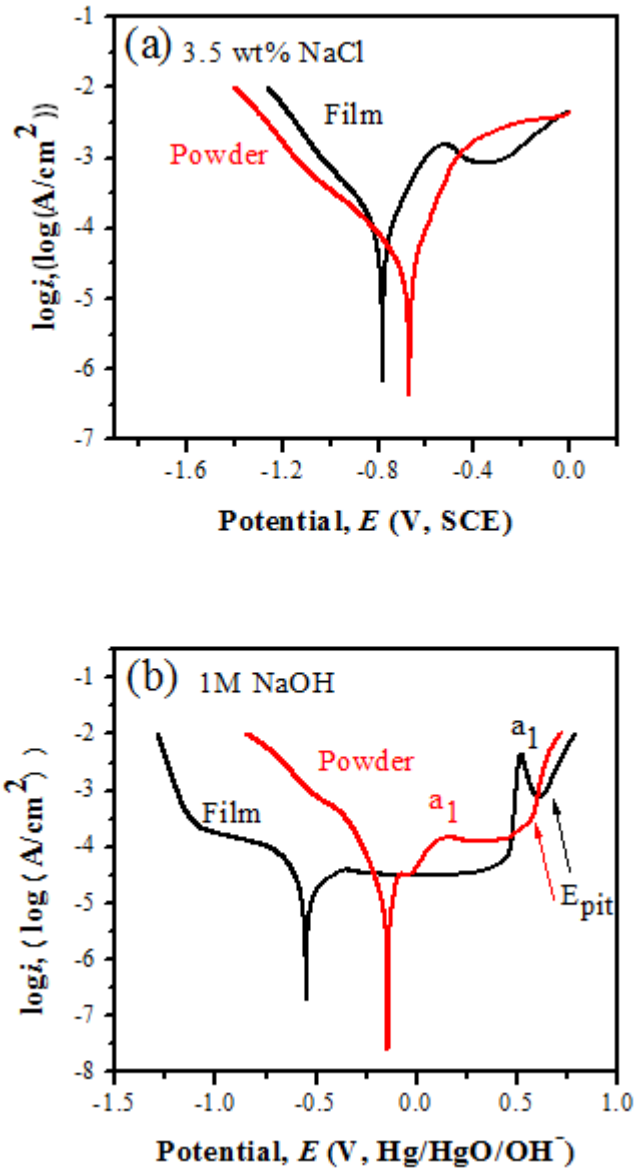

Figure 4. Potentiodynamic polarization curves of studied samples in (a) 3.5 wt% NaCl solution, (b) 1 M NaOH solution (scan rate: 5 mV/s).

The film sample has a current plateau i.e. passivation phenomenon, in the width of 0.3 V in the anodic part of the polarization curve, which is absent in the case of powder sample (Fig. 4a). Passivity can be explained according to the thickening of a P-enriched surface layer and the forming of $Ni(OH)_2$ that acts as the diffusion barrier for the dissolution of both components [24, 25]. In 1 M NaOH

solution, the E_{corr} of powder sample is -0.14 V, more positive than the film sample and similar to the situation in 3.5 wt% NaCl solution. Both samples have a current plateau and a peak denoted as a_1 in the anodic parts. The a_1 of powder sample at 0.25 V is more gently and occurs earlier than the film sample (Fig. 4b). According to our earlier argument [26], the peak at 0.5 V is attributed to the destruction of passive film. The damage of passive film is companied with the come off of fragments into solution, and then the combination of OH^- and Ni into new passive film resulting the decrease of current density. There are visible Tafel regions in the cathodic polarization sides in Fig. 4. Hence, we can use the curves of cathodic polarization sides to obtain the kinetic parameters of corrosion such as corrosion current density (i_{corr}), cathodic Tafel slope (β_c) and polarization resistance (R_p). The corrosion potential (E_{corr}) with the polarization kinetic parameters (β_c, R_p and i_{corr}) deduced from Fig. 4 are summarized in Table 2. The corrosion potential (E_{corr}) with the polarization kinetic parameters (i_{corr} and R_p) deduced from Fig. 4 are summarized in Table 2. In both solutions, the i_{corr} of powder sample is lower than that of film sample. In addition, R_p of powder sample is higher than film in both neutral and alkaline solution. These data indicate the resistance of powder sample is higher than film sample, which is consisted with their E_{corr} variation [27]. In 3.5 wt% NaCl solution, the β_c of the powder sample is very close to that of film sample, while the β_c of the powder sample is lower than that of film sample, showing a different changing behaviour from that in former solution, which is valuable to further study.

Table 2. Corrosion potential (E_{corr}), corrosion current density (i_{corr}), polarization resistance (R_p) and cathodic Tafel slope (β_c) calculated from polarization test in 3.5 wt% NaCl solution and 1 M NaOH solution of powder and film samples.

Solution	Electrodes	E_{corr} (V)	i_{corr} ($10^{-5}Acm^{-2}$)	R_p (Ωcm^2)	β_c (V/dec)
3.5% NaCl	Powders	-0.66	3.1	1100	0.20
	Film	-0.78	10.0	403	0.19
1 M NaOH	Powders	-0.14	2.0	2807	0.11
	Film	-0.54	3.9	2151	0.20

Moreover, the i_{corr} of each sample in NaCl solution is higher than in NaOH solution, which is corresponding with the larger R_p and larger E_{corr} in alkaline solution, because OH^- is more inactive than Cl^-.

Fig. 5 gives the SEM images of Ni–P alloys after potentiodynamic polarization in 3.5 wt% NaCl and 1 M NaOH solutions. In 3.5 wt% NaCl solution, the powder sample fork like cracks on the dense base and the powder aggregates of surface powders are distinctly separated. (Fig. 5a), and film sample have some micro cracks besides the pits in size of less than 1 μm (Fig. 5b). EDS analysis shows that the phosphorus content of powder sample and film is 15.5 % and 9.5 %, respectively. In 1 M NaOH solution, the crakes in the powder sample are more developed than that in NaCl solution

(Fig. 5c) and the dense base are frizzled. The cracks in the film sample is much more developed than that in NaCl solution (Fig. 5d), which agrees with the sharp peak a_1 in the polarization curve (Fig. 4b) according to our earlier argument [26]. Moreover, EDS analysis also shows that the phosphorus content of powder sample and film is 13.5 % and 8.4 %, which is consistent with the phenomena in NaCl solution and before polarization (Fig. 2).

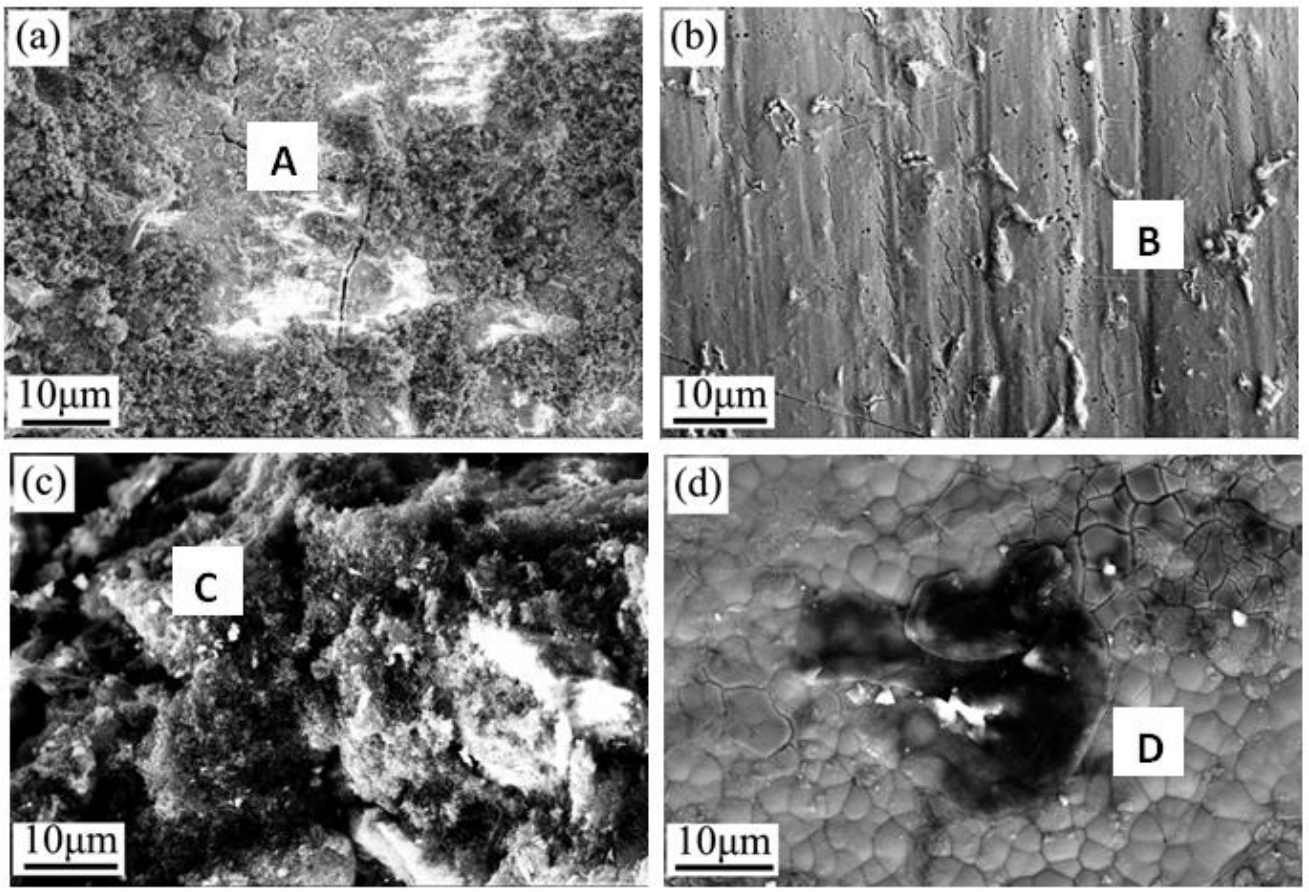

Figure 5. (a and b) SEM images of powder and film samples after potentiodynamic polarization test in 3.5 wt% NaCl solution and in (c and d) 1 M NaOH solution. EDS of A point: c_P = 15.5 at%, B point: c_P = 9.5 at%. C point: c_P = 13.5 at%, D point: c_P = 8.4 at%.

3.3. EIS measurement

The Nyquist plots of the powder sample and film in EIS measurements are shown in Fig. 6. The capacitive loop of the Ni–P powders is much larger than that of film.

For both samples, the most suitable model can be expressed by an equivalent circuit ($R_s(Q_f(R_f(Q_dR_t))))$ (the inset in Fig. 6) consisting of two parallel *RQ*s arrangement in series with the ohmic resistance and the mathematical expression of the impedance is shown in Eq. (1).

$$Z = R_s + \frac{1}{j\omega Q_f + \frac{1}{R_f + 1/\left(j\omega Q_d + (1/R_t)\right)}} \quad (1)$$

where R_s is the solution resistance, Q is the constant phase element (CPE). R_t is the charge-transfer resistance, Q_d is the nonideal double layer capacity, Q_f and R_f relate to the surface film features. Here, the pure capacity, C_x was replaced by the constant phase element, Q_x. It is used to present the distribution of relaxation times, as a capacitive element to consider the deviations of the system from the ideality [28, 29]. The impedance of the CPE, can be defined by:

$$Z_{CPE} = \frac{1}{(j\omega Q)^n} \quad (2)$$

where n is a fitted parameter, which is associated with the extent of dispersion attributing to the surface inhomogeneity. Hence, for a CPE, the exponent n is less than one and for the ideal case C, the perfect capacitor $n = 1$.

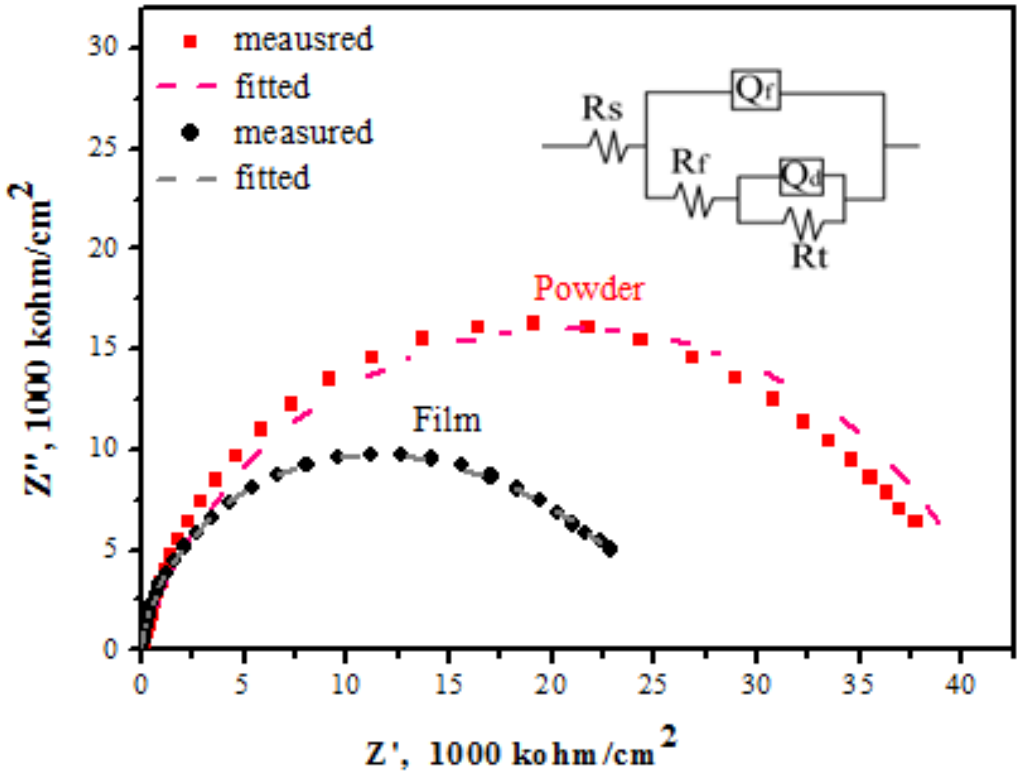

Figure 6. Nyquist plots and equivalent circuit model ($R(Q(R(QR))))$ used to analysis the EIS data of studied electrodes in 1M NaOH solution (scan rate: 5 mV/s).

In Eq. (1), the impedance Z is the transfer function of multiple variables (i.e., R_f, R_t, R_s Q_f, Q_d and ω). Whereas, once the parameters are determined by modeling, the impedance Z is a function of frequency ω, which generates an EIS spectrum. Moreover, the corrosion current density (i'_{corr}) at E_{corr} can be calculated from the impedance data [30] by:

$$i'_{corr} = \frac{RT}{FnR_t} \quad (3)$$

where R is the gas constant, F is the constant of Faraday, n is the fitting parameter of Q_f in Eq. (2), and T is the temperature.

The fitted parameters with the equivalent circuit model as well as i'_{corr} deduced from Eq. (3) are listed in Table 3. As is shown in Table 3, the charge transfer resistance R_t is much larger than other resistance values (R_s and R_f) for both powder and film samples.

Table 3. Impedance parameter values of charge-transfer resistance (R_t), solution resistance (R_s), film resistance (R_f), surface oxide film capacitance (Q_f), nonideal double layer capacitance (Q_d), and corrosion current density (i'_{corr}) of the powder and film samples in 1 M NaOH solution after holding the samples at open circuit potentials (OCP) for 2 h.

Samples	R_s (Ωcm^2)	Q_f (10^{-6} Fcm^{-2})	n_1 (0-1)	R_f (Ωcm^2)	Q_d (10^{-5} Fcm^{-2})	n_2 (0-1)	R_t (Ωcm^2)	i'_{corr} (10^{-5} Acm^{-2})
Powders	5.76	2.9	0.84	4.9	2.7	0.83	41510	0.07
Film	5.75	11.0	0.62	12.1	2.5	0.94	25210	0.10

Hence, the charge-transfer resistance is the dominant parameters of the corrosion process, which is similar to the work of Meng et al. [27, 31]. The R_t of powder sample is obviously higher than film and the i_{corr} of powder sample is lower than film, which means the stronger corrosion resistance ability of powder sample, and agrees with polarization curves. In addition, the larger n_1 and smaller Q_f of the powder sample indicate the formation of oxidation film in the electrode surface of powder sample is more easier than that of film. The reactions in an alkaline environment can result in localized precipitation of hydrated oxides (for example $Ni(OH)_2$) [32, 33]. In other words, the protection $Ni(OH)_2$ film formed more easily in powder sample than in the film sample.

3.4. Passive layer Mott-Schottky Analysis

In order to research the electronic properties of passivation films, the Mott-Schottky tests were carried out and shown in Fig. 7.

We can observe the slops in the linear region of the Mott-Schottky plot for two samples are opposite, one is positive and another is negative, which present an interesting phenomenon that the passive film of powder and film samples are n-type and p-type, respectively. The linear part of the Mott-Schottky relationship for n-type and p-type semiconductor is described by Ter-Ovanessian et al. [29, 34-36]:

$$C^{-2} = C_{SC}^{-2} = \frac{2}{\varepsilon\varepsilon_0 e N_D}\left(E - E_{FB} - \frac{kT}{e}\right) \text{ for n-type semiconductor} \quad (4)$$

$$C^{-2} = -C_{SC}^{-2} = -\frac{2}{\varepsilon\varepsilon_0 e N_A}\left(E - E_{FB} - \frac{kT}{e}\right) \text{ for p-type semiconductor} \quad (5)$$

where C is the measured capacitance, C_{sc} is the capacitance of the space-charge, E is the applied potential, E_{FB} is the flatband potential, k is the Boltzmann constant, N_D and N_A are the donor

density and acceptor density, respectively and *e* is the electron charge. Assuming that at the passive film/electrolyte interface, region is lower than that of the double layer and the latter capacitance can be neglected. N_D and N_A can be calculated by the slope of C_{SC}^{-2} vs. E and E_{FB} can be obtained by extrapolation to C_{SC}^{-2} = 0 on the potential axis. Because the CPE behaviour was observed in electrochemical impedance spectroscopy curves (Fig. 6), the measured capacitance is frequency-dependent [35, 37]. The calculated E_{FB} and the donor density N_D and acceptor density N_A for powder sample and film can be seen in Fig. 7.

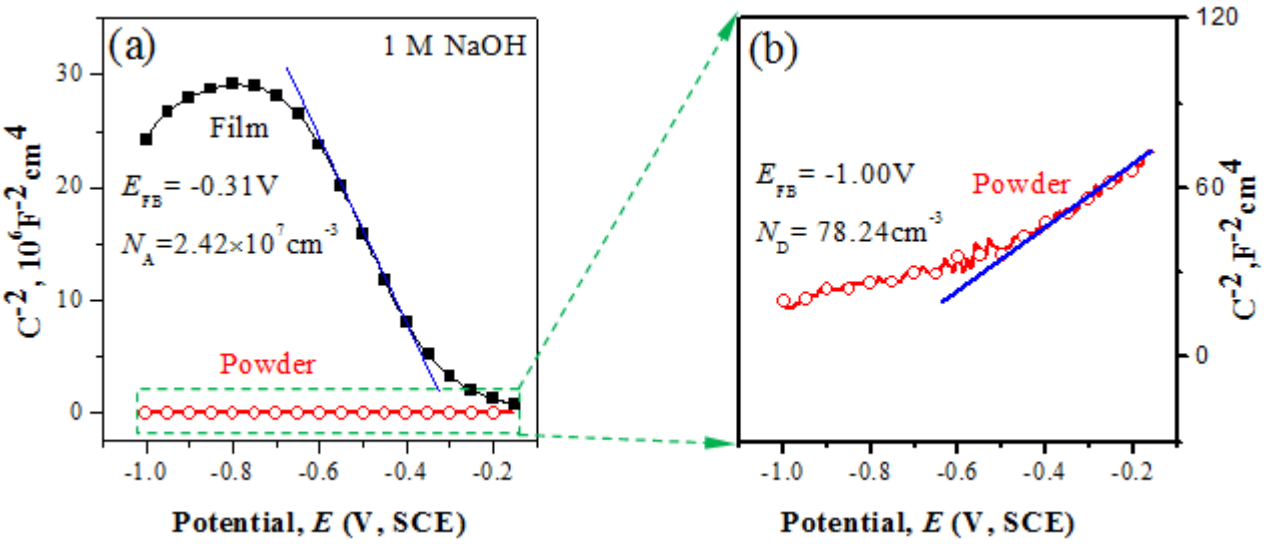

Figure 7. Mott-Schottky relationships of (a) powder and film samples; (b) magnification of film obtained at 1000 Hz in 1 M NaOH solution (scan rate: 5 mV/s).

In Fig. 7, the E_{FB} of powder sample is obviously higher than film. This phenomenon is related to the energy level of semiconductor, two reactions generate in two different energy levels, which are valence band and conduction band with the corresponding powder sample and film sample. And the energy level of conduction band is higher than that of valence band in semiconductor energy band model [35, 38]. The higher energy band means that electron needs more energy to realize transition.

Meanwhile, the doner density N_D of the powder sample is lower than the acceptor density N_A of film sample, indicating a lower charge carrier concentration, a lower disordered in passive film and a lower conductivity of powder sample, and there exist a corresponding between Mott-Schottky test, the EIS test and the Tafel test in the works of Freire et al. [14]. Generally, passive films formed on Ni–P samples are consisted of a lot of hydroxides or of a significant hydrated layer (NiO/NiOOH) which may generate the high values of charge carries [34]. The Mott-Schottky results are corresponding to higher R_t of powder sample in EIS test (Table 3).

3.5. Cyclic voltammetry of Ni–P samples

Fig. 8 compares the cyclic voltammograms (CV) of powder and film samples in various solutions recorded at a potential sweep rate of 5 mV/s. The anodic part of CV curves of both samples is similar to their polarization curves. Bode et al. [39] demonstrated that at least two nickel hydroxides (such as α- and β-$Ni(OH)_2$) and two hydrous oxides (like β- and γ-NiOOH) are electrochemically formed, each with distinguishable electrochemical properties and crystalline microstructure [6, 40]. The cathodic charge densities (q_c, area above the peak α'_1) of the powder sample is approximately lower than the anodic charge densities (q_a, area below the peak α_1).

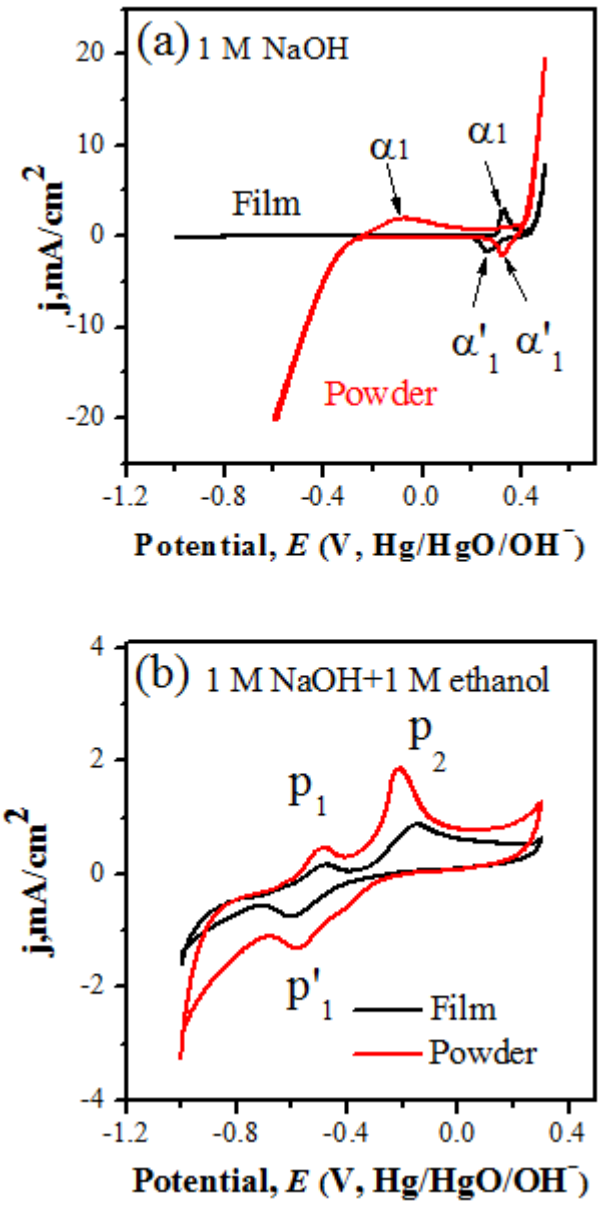

Figure 8. Cyclic voltammograms of studied electrodes with the potential range of -1.2 to 0.6 V in (a) 1 M NaOH solution, (b) 1 M NaOH in the presence of 1 M ethanol solution.

The q_c, area above the peak α'_1 of the film sample is approximately equal to the q_a, area below the peak α_1 in Fig. 8a, demonstrating a good reversibility of the redox reaction, which is similar to the work of Kang et al. [40]. Many researchers suggested the presence of reversible process of

$$Ni \rightarrow Ni(OH)_2 \quad (6)$$

for Ni–P electrodes in alkaline solution in a low potential ranges. Comparison of the cyclic voltammogram with pure nickel and Ni–P electrodes in alkaline solutions shows that peak α_1 may be assigned to the adsorption of OH^- and simultaneous oxidation of Ni to α- $Ni(OH)_2$. Besides, conversion of α- $Ni(OH)_2$ to a more stable β- $Ni(OH)_2$ may occur in this region. The cathodic peak α'_1 is connected with the reduction of high valence nickel oxides $Ni(OH)_2$ back to Ni [12, 18].

The area of anodic peak α_1 of powders electrode is larger than the cathodic peak α'_1. It is reasonable to suggest that the reaction of Eq. (6) is accompanied by another anodic process. As the work of Kang et al. [40], both elemental P and phosphide exist in a fresh Ni–P alloy sample. We can deduce that in the potential region P is oxidized. The reasonable reaction may be described as following form [6]:

$$P + 8OH^- = PO_4^{3-} + 4H_2O + 5e^- \quad (7)$$

The potential and area of cathodic peak α'_1 of Ni–P powders electrode are similar to those of Ni–P film electrode α'_1. Therefore, the reaction attributed to peak α'_1 is the same as the reaction for film: $Ni(OH)_2$/Ni.

In the alkaline solution with the addition of ethanol, there exist two peaks P_1 and P_2 in the anodic part of CV curves of the powder sample (Fig. 8b). The peak p_1 at -0.5 V locates earlier than the peak α_1 in NaOH solutions, and should be ascribed to Ni/α- $Ni(OH)_2$ conversion and other peak p_2 at -0.2 V is allocated to the α-$Ni(OH)_2$/β-$Ni(OH)_2$ conversion and β-$Ni(OH)_2$/NiOOH oxidation process [18, 41, 42]:

$$\alpha - Ni(OH)_2 \rightarrow \beta - Ni(OH)_2 \quad (8)$$

$$\beta - Ni(OH)_2 + OH^- \rightarrow NiOOH + H_2O + e^- \quad (9)$$

In the anodic direction, NiOOH served as a strong oxidizing agent and Ni^{3+} sites are regenerated by the power source and used as active surface for ethanol oxidation [18, 42, 43]:

$$NiOOH + RCH_2OH \rightarrow Ni(OH)_2 + RC\cdot HOH \quad (10)$$

$$RC\cdot HOH + 3OH^- \rightarrow RCOOH + 2H_2O + 3e^- \quad (11)$$

here, R refers to the functional group $–CH_2$ of enthanol.

The main difference between the cyclic voltammograms of powder and film samples is that the peak areas of the powder sample are obviously bigger than those of film sample (Fig. 8b). The higher anodic peaks demonstrate that more low valence Ni can be oxidized to Ni^{2+} ($Ni(OH)_2$) in the powder sample. On the other hand, the powder sample can serve as substrate in catalytic process and maybe supply more activity oxidation sites Ni^{3+} than the film sample, which is attributed to its unique porous microstructure with a larger special surface area, according to the argument in Azizi et al. [18, 43, 44]. At the same time, the cathodic peak P'_1 current intensity (assigned to NiOOH reduction) of the powder sample is higher compared with the film sample in Fig. 8b. As a result, more NiOOH could be reduced and subsequently the intensity of cathodic peak P'_1 increases according to a higher electrocatalytic

activity toward ethanol oxidation [6]. These results indicate that the powder sample own a higher electrocatalytic activity toward ethanol oxidation than the film sample.

4. CONCLUSIONS

Amorphous Ni–P prepared by electroless method into two different forms respectively is powders and thin films by two different substrates. In microstructure aspects, the powder sample owning a porous microstructure, which have the more amorphous characteristic compared with the film using XRD and TEM. The corrosion behaviour of the samples was examined using potentiodynamic polarization test and electrochemical impedance spectroscopy (EIS). The potentiodynamic polarization analysis shows that the powder sample had a higher corrosion resistance than film sample. The polarization resistance R_p and electrochemical transfer resistance R_t (deduced from EIS) of the powder sample are obviously higher than these of the film sample. Ni–P powders and film present two different types of semiconductor in the surface of passive films and powder sample own a lower donor density N_D according to the Mott-Schottky tests, which agrees well with the results of Tafel tests and EIS tests. Cyclic voltammetry indicate that the powder sample exhibits significantly higher catalytic activity for electro-oxidation of ethanol, which is possibly ascribed to its higher R_t and N_D.

ACKNOWLEDGMENTS
The work is supported by National Natural Science Foundation of China (No.51171091 and No.51471099), and National Basic Research Program of China (973Program) (No.2012CB825702).

References

1. J.N. Balaraju, K.S. Rajam, *Int. J. Electrochem. Sci.*, 2 (2007) 747-761.
2. S.L. Ye, X.Y. Li, X.F. Bian, W.M. Wang, L.J. Yin, B. An, *J. Alloy. Compd.*, 562 (2013) 143-149.
3. C. Domínguez-Ríos, A. Hurtado-Macias, R. Torres-Sánchez, M.A. Ramos, J. González-Hernández, *Ind. Eng. Chem. Res.*, 51 (2012) 7762-7768.
4. N. Nwosu, A. Davidson, C. Hindle, M. Barker, *Ind. Eng. Chem. Res.*, 51 (2012) 5635-5644.
5. C.O. Osifuye, A.P.I. Popoola, C.A. Loto, D.T. Oloruntoba, *Int. J. Electrochem. Sci.*, 9 (2014) 6074-6087.
6. A.M. Fundo, L.M. Abrantes, *J. Electroanal. Chem.*, 600 (2007) 63-79.
7. H.X. Li, W.J. Wang, H. Li, J.F. Deng, *J. Catal.*, 194 (2000) 211-221.
8. H. Li, H.X. Li, W.L. Dai, W.J. Wang, Z.G. Fang, J.F. Deng, *Appl. Surf. Sci.*, 152 (1999) 25-34.
9. V. Vitry, A.F. Kanta, F. Delaunois, *Ind. Eng. Chem. Res.*, 51 (2012) 9227-9234.
10. K. Lu, W.D. Wei, J.T. Wang, *Scripta Mater.*, 24 (1990) 2319-2323.
11. K.H. Krishnan, S. John, K.N. Srinivasan, J. Praveen, M. Ganesan, P.M. Kavimani, *Metall. Mater. Trans. A*, 37 (2006) 1917-1926.
12. R.K. Shervedani, A. Lasia, *J. Electrochem. Soc.*, 144 (1997) 511-519.
13. Z.H. Xie, G. Yu, B.N. Hu, X.Y. Zhang, L.B. Li, W.G. Wang, D.C. Zhang, *Int. J. Electrochem. Sci.*, 8 (2013) 6664-6677.
14. L. Freire, M.J. Carmezim, M.G.S. Ferreira, M.F. Montemor, *Electrochim. Acta*, 55 (2010) 6174-

6181.
15. J.F. Deng, H.X. Li, W.J. Wang, *Catal. Today*, 51 (1999) 113-125.
16. X.G. Wang, W.M. Wang, Z. Qi, C.C. Zhao, H. Ji, Z.H. Zhang, *Electrochem. Commun.*, 11 (2009) 1896-1899.
17. M.L. Helm, M.P. Stewart, R.M. Bullock, M.R. DuBois, D.L. DuBois, *Science*, 333 (2011) 863-866.
18. S.N. Azizia, S. Ghasemi, F. Amiripour, *Electrochim. Acta*, 137 (2014) 395-403.
19. R.M.A. Hameed, K.M. El-Khatib, *Int. J. Hydrogen. Energ*, 35 (2010) 2517-2529.
20. M. Fleischmann, K. Korinek, D. Pletcher, *J. Chem. Soc., Perkin Trans. 2*, (1972) 1396-1403.
21. E. Georgiza, J. Novakovic, P. Vassiliou, *Surf. Coat. Technol.*, 232 (2013) 432-439.
22. H.S. Yu, S.F. Luo, Y.R. Wang, *Surf. Coat. Technol.*, 148 (2001) 143-148.
23. L.L. Meng, X.Y. Li, J. Pang, L. Wang, B. An, L.J. Yin, K.K. Song, W.M. Wang, *Metall. Mater. Trans. A*, 44 (2013) 5122-5133.
24. P. em., D.r. nat., H. Kaesche, *Corrosion of Metals*, Springer Berlin Heidelberg, Berlin Heidelberg (2003).
25. C.K. Lee, *Mater. Chem. Phys.*, 114 (2009) 125-133.
26. G.H. Li, S.P. Pan, J.Y. Qin, Z.H. Zhang, W.M. Wang, *Corros. Sci.*, 66 (2013) 360-368.
27. Q.G. Meng, J.G. Li, X.F. Bian, *J. Alloy. Compd.*, 424 (2006) 350-355.
28. J.R. Macdonald, *J. Electroanal. Chem.*, 223 (1987) 25-50.
29. C.N. Cao, *Corrosion Electrochemistry*, Chemical Industry Press, Beijing (1985).
30. J.P. Diard, B. Le-Gorrec, C. Montella, *J. Electroanal. Chem.*, 326 (1992) 13-36.
31. F. Mansfeld, *Electrochim. Acta*, 35 (1990) 1533-1544.
32. M.F. Montemor, A.M. Sim˜ oes, M.G.S. Ferreira, *Prog. Org. Coat.*, 43 (2001) 274-281.
33. N. Mora, E. Cano, J.L. Polo, J.M. Puente, J.M. Bastidas, *Corros. Sci.*, 46 (2004) 563-578.
34. B. Ter-Ovanessian, C. Alemany-Dumont, B. Normand, *Electrochim. Acta*, 133 (2014) 373-381.
35. J.Q. Zhang, *Electrochemical Measurement Technology*, Chemical Industry Press, Beijing (2010).
36. S. Ningshen, U. Kamachi Mudali, V.K. Mittal, H.S. Khatak, *Corros. Sci.*, 49 (2007) 481-496.
37. W. Wang, A. Alfantazi, *Electrochim. Acta*, 131 (2014) 79-88.
38. Morrison, R. Stanley, *Electrochemistry at semiconductor and oxidized metal electrodes*, Plenum Press, New York (1980).
39. H. Bode, K. Dehmelt, J. Witte, *Electrochim. Acta*, 11 (1966) 1079-1087.
40. J.Q. Kang, Y.F. Yang, H.X. Shao, *Corros. Sci.*, 51 (2009) 1907-1913.
41. Q.F. Yi, J.J. Zhang, W. Huang, X.P. Liu, *Catal. Commun.*, 8 (2007) 1017-1022.
42. A. Ehsani, M.G. Mahjani, M. Jafarian, A. Naeemy, *Electrochim. Acta*, 71 (2012) 128-133.
43. H.C. He, P. Xiao, M. Zhou, Y.H. Zhang, Q. Lou, X.Z. Dong, *Int. J. Hydrogen. Energ*, 37 (2012) 4967-4973.
44. R.C. Sekol, M. Carmo, G. Kumar, F. Gittleson, G. Doubek, K. Sun, J. Schroers, A.D. Taylor, *Int. J. Hydrogen. Energ*, 38 (2013) 11248-11255.